

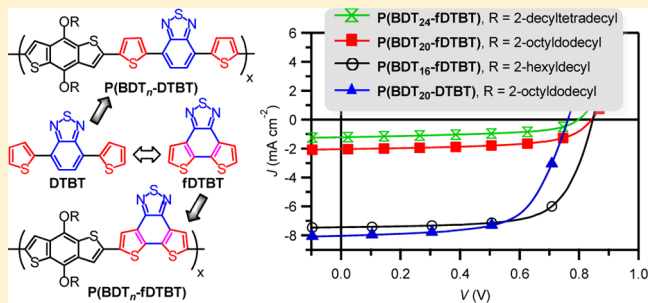
A Family of Donor–Acceptor Photovoltaic Polymers with Fused 4,7-Dithienyl-2,1,3-benzothiadiazole Units: Effect of Structural Fusion and Side Chains

Chong-Yu Mei,* Long Liang, Fu-Gang Zhao, Jin-Tu Wang, Lin-Feng Yu, Yu-Xue Li,* and Wei-Shi Li*

Shanghai Institute of Organic Chemistry, Chinese Academy of Sciences, 345 Lingling Road, Shanghai 200032, China

Supporting Information

ABSTRACT: A new optoelectronic building block, dithieno[3',2':3,4;2'',3'':5,6]benzo[1,2-*c*][1,2,5]thiadiazole, was designed by applying a fusion strategy on 4,7-dithienyl-2,1,3-benzothiadiazole (DTBT) and named as fDTBT. In combination with benzo[1,2-*b*:4,5-*b'*]dithiophene (BDT), fDTBT was used for the construction of a family of donor–acceptor copolymers, P(BDT_n-fDTBT), with different side chains (*n* is carbon number of the side chain and varies from 8, 10, 12, 16, 20, to 24). It was found that the side chains have great impact on processing and photovoltaic properties of the polymers. P(BDT_n-fDTBT) (*n* = 8, 10, and 12) bearing small alkyl side chains show poor solubility even in hot solvents. P(BDT_n-fDTBT) (*n* = 20 and 24) have good solubility but inferior photovoltaic performance with an efficiency of 1.04% and 0.49%, respectively. Only P(BDT₁₆-fDTBT) having 2-hexyldecyl side chain possesses both suitable solution processability and good photovoltaic properties with an efficiency around 4.36%. The comparison between P(BDT₁₆-fDTBT) with the nonfused reference polymer P(BDT₂₀-DTBT) reveals that the structural fusion on DTBT endows the polymer a deeper HOMO energy level and a better film morphology when blending with [6,6]-phenyl-C₆₁-butyric acid methyl ester (PC₆₁BM), finally resulting in improved photovoltaic performance.



1. INTRODUCTION

Organic solar cells (OSCs) have attracted increasing attention due to their active layer based on lightweight, designable, synthesized, and solution-processable organic semiconductors.¹ In the past few years, the power conversion efficiency (PCE) of OSCs has progressively improved and surpassed 7% for a single junction device,^{2–6} making them more realistic to be a complement or even an alternative to silicon-based solar electric generation technology. However, for their commercial use, this efficiency level is still low and must be further increased.

The history of OSCs tells us material innovation is one of the important driving forces in the field. In the early era of OSCs, poly(phenylenevinylene)s (PPVs) and polythiophenes (PTs) were two kinds of typical electron-donating materials that dominated organic photovoltaic (OPV) researches.⁷ Especially, poly(3-hexylthiophene) (P3HT) has represented a top-excellent material. Bulk heterojunction (BHJ) devices based on its blend with [6,6]-phenyl-C₆₁-butyric acid methyl ester (PC₆₁BM) have achieved a PCE of 4–5%.⁸ However, it suffers from two shortages: (1) the light acquisition capability limited to 650 nm; (2) a high-lying highest occupied molecular orbital (HOMO). Since the structure composed of alternative electron-donating (D) and -accepting (A) units can lower the energy gap and enable a more efficient light harvesting in the far visible and even near-infrared region, a variety of D–A copolymers have been designed and synthesized to replace

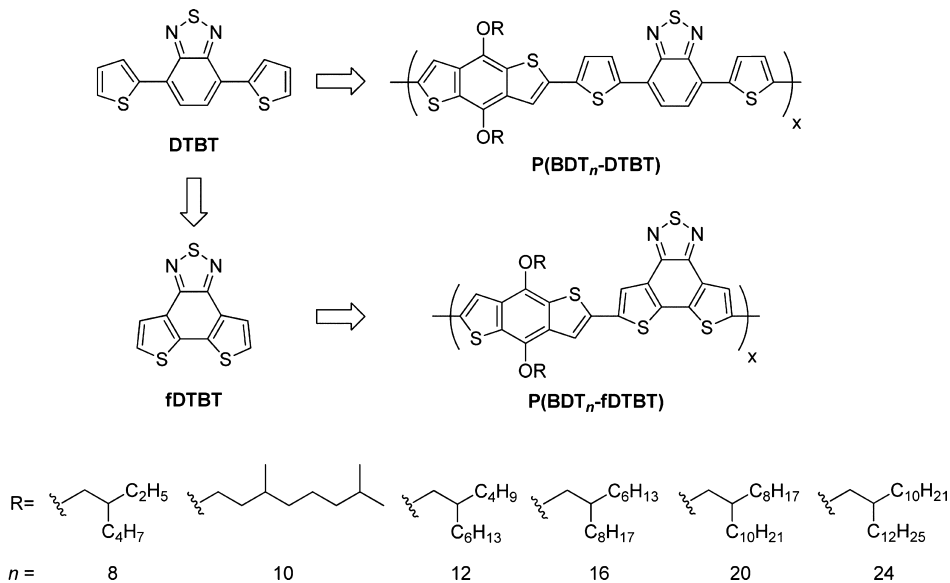
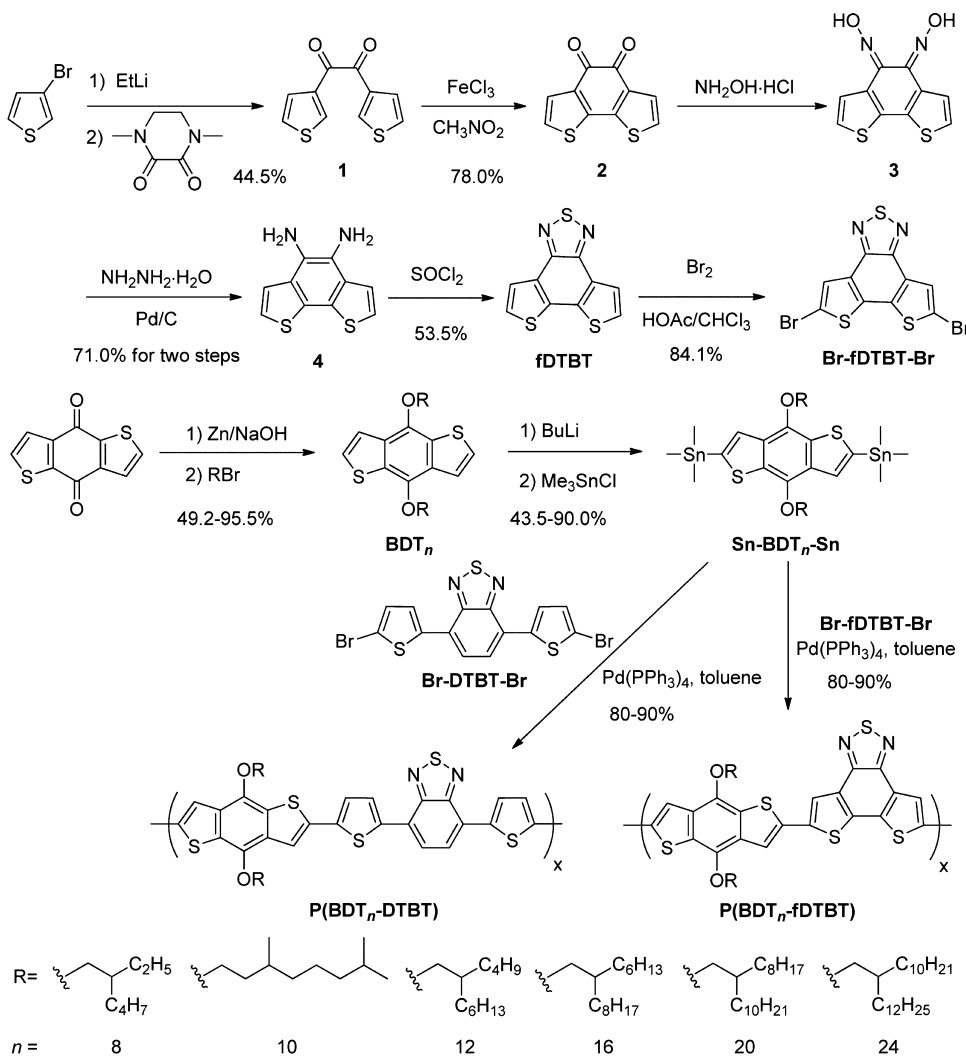
P3HT.^{1,9} Some of them, such as poly(thienothiophene-*alt*-benzodithiophene) (PTB),² poly(dithienosilole-*alt*-thienopyrrole-4,6-dione) (PDTSTPD),³ poly(benzodithiophene-*alt*-dithienyldifluorobenzothiadiazole) (PBnDT-DTffBT),⁴ and poly(dithienogermole-*alt*-thienopyrrolodione) (PDTGTPD),⁵ have achieved a PCE over 7%. After integrating a polyelectrolyte layer into device configuration, the cells based on the blend of PTB/PC₇₁BM exhibited a champion PCE record of 9.2% among the present reported single-junction OSCs.^{2c}

In the design of new optoelectronic moieties for D–A copolymers, fusion and planarization are effective and popular approaches.¹⁰ These approaches often produce large fused polycyclic aromatic units, which can suppress interannular rotation, allow better π -electron delocalization, enhance intermolecular interactions, and thus may improve the properties of light absorption and charge transportation. One famous example is poly(fluorenedicyclopentathiophene-*alt*-benzothiadiazole) (PFDCTBT),⁶ which is the analogue of poly(2,7-fluorene-*alt*-dithienylbenzothiadiazole) (PFDTBT). The OPV cells based on PFDTBT showed a PCE in the range of 1–4%.¹¹ After planarization, PFDCTBT exhibited notably increased photovoltaic performance with a high field-effect hole mobility and a high PCE (7% for the best). Other

Received: June 23, 2013

Revised: September 15, 2013

Published: September 26, 2013

Chart 1. Molecular Structures of DTBT, fDTBT, Copolymer P(BDT_n-DTBT), and P(BDT_n-fDTBT)Scheme 1. Synthesis of fDTBT and Its Copolymer P(BDT_n-fDTBT) ($n = 8, 10, 12, 16, 20$, and 24), and the Reference Polymer P(BDT_n-DTBT) ($n = 16$ and 20)

examples including bridged thiophene–phenylene–thiophene,¹² diindenothieno[2,3-*b*]thiophene,¹³ and ladder-type nonacyclic thienyl–phenylene–thienylene–phenylene–thienyl unit,¹⁴ showed promising photovoltaic properties.

In this work, we applied fusion strategy on 4,7-dithienyl-2,1,3-benzothiadiazole (DTBT, Chart 1), a well-known building block for D–A photovoltaic copolymers. In 2003, Andersson et al. first reported the use of DTBT for D–A copolymers, in which it was combined with fluorene unit to produce the above-mentioned PFDTBT.^{11a} PFDTBT exhibited a deep-lying HOMO energy level and achieved an impressive large open circuit voltage (V_{OC}) of around 1 V and a PCE of 4.5% when blending with PC₇₁BM.^{11d} In 2007, Leclerc and co-workers reported PCDTBT, which contains DTBT and carbazole units.¹⁵ The OPV cells based on this polymer and PC₇₁BM displayed outstanding performance with a PCE over 6%.¹⁶ In addition to fluorene and carbazole units, a variety of electron-donating moieties including dibenzosilole,¹⁷ dithienopyrrole,¹⁸ indolo[2,3-*b*]carbazole,¹⁹ and ladder-type oligo-*p*-phenylene²⁰ have also been utilized to integrate with DTBT. The most produced D–A copolymers showed photovoltaic properties having a PCE in the range of 2–6%. Inspired by these works, we envisioned that the direct fusion of the two end thienyl units into the central benzothiadiazole would produce a new planar polycyclic aromatic unit, dithieno-[3',2':3,4;2'',3'':S,6]benzo[1,2-*c*][1,2,5]thiadiazole, and it would be a new promising building block for novel photovoltaic D–A copolymers (Chart 1). Since it is a fused version of DTBT, we named this unit fDTBT in the following context. Here, we report its synthesis and the combination with benzo[1,2-*b*:4,5-*b'*]dithiophene (BDT) unit for the preparation of D–A copolymers, P(BDT_{*n*}-fDTBT) (*n* is the carbon number of R, the side chain on BDT). In order to investigate the effect of structural fusion, we also prepared reference polymers P(BDT_{*n*}-DTBT)²¹ based on DTBT and BDT and compared their properties under same conditions. We found P(BDT_{*n*}-fDTBT) polymers possess a lower HOMO energy level than P(BDT_{*n*}-DTBT), thus enabling a larger V_{OC} and finally better photovoltaic performance. We also highlight that the side chains (R on BDT unit, Chart 1) have great impact on the physical and photovoltaic properties of the polymers, in which an appropriate alkyl size is essential to ensure the polymer to possess both processable solubility and good photovoltaic performance.

2. RESULTS AND DISCUSSION

Synthesis and Thermal Stability. The synthesis of fDTBT is depicted in Scheme 1. The important diketone intermediate (compound 2) was prepared from 3-bromothiophene via three steps: metalation with EtLi, then reaction with 1,4-dimethylpiperazine-2,3-dione, followed by intramolecular thiophene–thiophene coupling with FeCl₃.²² After condensation with hydroxylamine in a mixture solvent of ethanol and pyridine, diketone intermediate 2 was transferred into dioxime 3, which was directly reduced to diamine compound 4 by hydrazine under the catalysis of Pd/C. After treatment of compound 4 with freshly distilled thionyl chloride in the presence of triethylamine in dichloromethane, compound fDTBT was finally prepared in 53.5% yield. Bromination of fDTBT with bromine in acetic acid/chloroform produced compound Br-fDTBT-Br, one of the important monomers for the preparation of D–A copolymers, in 84.1% yield. Another important monomer, Sn-BDT_{*n*}-Sn, was synthesized following a

literature method.²³ The final D–A copolymers, P(BDT_{*n*}-fDTBT), were prepared via Stille-coupling polymerization between Br-fDTBT-Br and Sn-BDT_{*n*}-Sn in the presence of Pd(PPh₃)₄ in toluene for 48 h and purified by precipitation from methanol and subsequent Soxhlet extraction with methanol, acetone, hexane, chloroform, and chlorobenzene in sequence. During the extraction, we found that the solubility of the polymers greatly depends on their side chains. P(BDT₈-fDTBT), P(BDT₁₀-fDTBT), and P(BDT₁₂-fDTBT) with small alkyl side chains cannot dissolve in chloroform, chlorobenzene (CB), and *o*-dichlorobenzene (ODCB) and even in their hot state. P(BDT₁₆-fDTBT) with 2-hexyldecyl side chain is soluble in hot CB and ODCB, but not in hot chloroform, whereas P(BDT₂₀-fDTBT) can dissolve in chlorinated solvents, such as chloroform. Surprisingly, P(BDT₂₄-fDTBT) has a very good solubility, which was completely extracted by hexane. The polymer P(BDT_{*n*}-DTBT) were synthesized similarly but with Sn-BDT_{*n*}-Sn and bis(5-bromo-2-thienyl)-2,1,3-benzothiadiazole (Br-DTBT-Br) as monomers. P(BDT₁₆-DTBT) is also not processable, whereas P(BDT₂₀-DTBT) is soluble in hot ODCB. Since no solvent is applicable for P(BDT₈-fDTBT), P(BDT₁₀-fDTBT), P(BDT₁₂-fDTBT), and P(BDT₁₆-DTBT), the later studies were focused only on P(BDT₁₆-fDTBT), P(BDT₂₀-fDTBT), P(BDT₂₄-fDTBT), and P(BDT₂₀-DTBT).

The soluble polymers were characterized by gel permeation chromatography (GPC). The measurements of P(BDT₂₀-fDTBT) and P(BDT₂₄-fDTBT) were performed with chloroform eluent at room temperature, while that of P(BDT₁₆-fDTBT) and P(BDT₂₀-DTBT) were carried out with 1,3,5-trichlorobenzene eluent at 150 °C, both using monodispersed polystyrenes as standards. The number-average molecular weight (M_n) and polydispersity index (PDI) were determined to be 29.7 kDa and 2.33 for P(BDT₁₆-fDTBT), 23.1 kDa and 1.65 for P(BDT₂₀-fDTBT), 27.1 kDa and 1.94 for P(BDT₂₄-fDTBT), and 31.7 kDa and 1.84 for P(BDT₂₀-DTBT) (Table 1). The data indicate that all four polymers have similar

Table 1. Molecular Weights and Thermal Stabilities of P(BDT_{*n*}-fDTBT) (*n* = 16, 20, and 24) and P(BDT₂₀-DTBT)

polymer	M_n (kDa)	M_w (kDa)	PDI	T_d ^c (°C)
P(BDT ₁₆ -fDTBT)	29.7 ^a	69.3 ^a	2.33 ^a	317.2
P(BDT ₂₀ -fDTBT)	23.1 ^b	38.2 ^b	1.65 ^b	314.8
P(BDT ₂₄ -fDTBT)	27.1 ^b	52.7 ^b	1.94 ^b	318.6
P(BDT ₂₀ -DTBT)	31.7 ^a	58.3 ^a	1.84 ^a	304.5

^aDetermined by GPC with 1,3,5-trichlorobenzene eluent at 150 °C using monodispersed polystyrenes as standards. ^bDetermined by GPC with chloroform eluent at room temperature using monodispersed polystyrenes as standards. ^c5% weight loss temperature.

molecular weight and polydispersity, which ensure a comparable basis to penetrate the effect of structural fusion and different side chains on their photophysical and photovoltaic properties. Thermogravimetric analysis (TGA, Figure 1) revealed that all four polymers possess similar thermal stability with a 5% weight loss temperature (T_d) over 300 °C, stable enough for their applications in OSCs and other optoelectronic devices. No obvious thermal transition was observed for all four polymers from 0 to 250 °C (Figure 2).

Optical Properties. The optical properties of polymer P(BDT_{*n*}-fDTBT) and P(BDT₂₀-DTBT) were analyzed by UV-vis spectroscopy in both solution and film states (Figure 3). In chlorobenzene solution, P(BDT₂₀-fDTBT) and P-

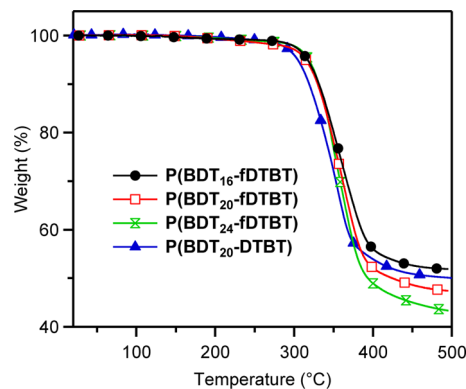


Figure 1. TGA curves of $P(BDT_n\text{-}fDTBT)$ ($n = 16, 20$, and 24) and $P(BDT_{20}\text{-}DTBT)$ with a heating rate of $10\text{ }^{\circ}\text{C min}^{-1}$ under nitrogen flow.

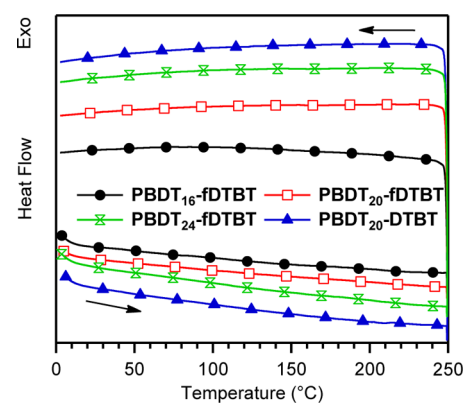


Figure 2. Second heating and cooling DSC traces of $P(BDT_n\text{-}fDTBT)$ ($n = 16, 20$, and 24) and $P(BDT_{20}\text{-}DTBT)$ with a heating rate of $10\text{ }^{\circ}\text{C min}^{-1}$ and a cooling rate of $15\text{ }^{\circ}\text{C min}^{-1}$ under nitrogen.

($BDT_{24}\text{-}fDTBT$) show identical UV-vis absorption spectra (Figure 3a), with two intense bands centered at 522 and 560 nm and two relatively weak peaks around 340 and 426 nm. These spectral features are similar to the reported BDT-containing D-A copolymers.²⁴ The peak at the longest wavelength is assignable to the intramolecular charge-transfer (ICT) transition between BDT and fDTBT units. Under the same conditions, $P(BDT_{16}\text{-}fDTBT)$ displays a similar UV-vis spectrum to those of $P(BDT_{20}\text{-}fDTBT)$ and $P(BDT_{24}\text{-}fDTBT)$ but with slightly red-shifted peaks (526 and 564 nm). In film

state, all the polymers show slightly red-shifted spectra from those in solution (Figure 3b). The maximum peaks of $P(BDT_{20}\text{-}fDTBT)$ and $P(BDT_{24}\text{-}fDTBT)$ appear at 564 nm, while that for $P(BDT_{16}\text{-}fDTBT)$ at 568 nm. The red shift observed in the spectrum of $P(BDT_{16}\text{-}fDTBT)$ referred to those of $P(BDT_{20}\text{-}fDTBT)$ and $P(BDT_{24}\text{-}fDTBT)$ in either solution or film state implies that the smaller side chain in $P(BDT_{16}\text{-}fDTBT)$ enables stronger $\pi\text{-}\pi$ interchain interactions and would do favor to charge transportation across the polymer chains. Surprisingly, $P(BDT_{16}\text{-}fDTBT)$ possesses larger absorption coefficients than other $P(BDT_n\text{-}fDTBT)$ in both solution and film state, which would be another beneficial factor for its photovoltaic application. Calculated from the absorption edges of their thin films (all around 614 nm), all three polymers have similar optical energy gap of 2.02 eV.

Since nonfused polymer $P(BDT_{20}\text{-}DTBT)$ cannot dissolve in chlorobenzene, *o*-dichlorobenzene was used for its UV-vis spectroscopy. As shown in Figure 3a, $P(BDT_{20}\text{-}DTBT)$ displays two significant absorption peaks with their maxima at 424 and 638 nm in solution. The peak at the longer wavelength is an ICT transition between BT and dithienyl BDT. In film state, this peak appears at 646 nm, 8 nm red-shifted from that in solution (Figure 3b). As compared with $P(BDT_n\text{-}fDTBT)$, $P(BDT_{20}\text{-}DTBT)$ exhibits a significant bathochromic-shifted ICT transition (>70 nm) either in solution or in film state. This fact suggests that the fusion of two electron-donating thiophenyl units into electron-deficient BT ring greatly reduces the electron-accepting property of the whole moiety. From its absorption edge in film state (~729 nm), the optical energy gap of $P(BDT_{20}\text{-}DTBT)$ was estimated to be 1.70 eV, 0.32 eV smaller than that of $P(BDT_n\text{-}fDTBT)$. The larger energy gap generally reduces photocurrent of OSC devices and would be one of the shortages for the fused polymers $P(BDT_n\text{-}fDTBT)$.

Electrochemical Properties. Electrochemical properties of the polymers were investigated via cyclic voltammetry (CV) using a three-electrode cell with a glass carbon working electrode, a platinum wire counter electrode, and an Ag/AgNO₃ reference electrode. The measurements were performed with film samples prepared by drop-casting their chlorobenzene or *o*-dichlorobenzene solutions onto a glass carbon electrode and carried out in an acetonitrile solution containing 0.1 M Bu₄NPF₆ at a scan rate of 50 mV s⁻¹.

Figure 4 displays the positive CV scanning profiles of $P(BDT_n\text{-}fDTBT)$ ($n = 16, 20$, and 24) and $P(BDT_{20}\text{-}DTBT}$). The polymer $P(BDT_n\text{-}fDTBT)$ shows irreversible oxidation

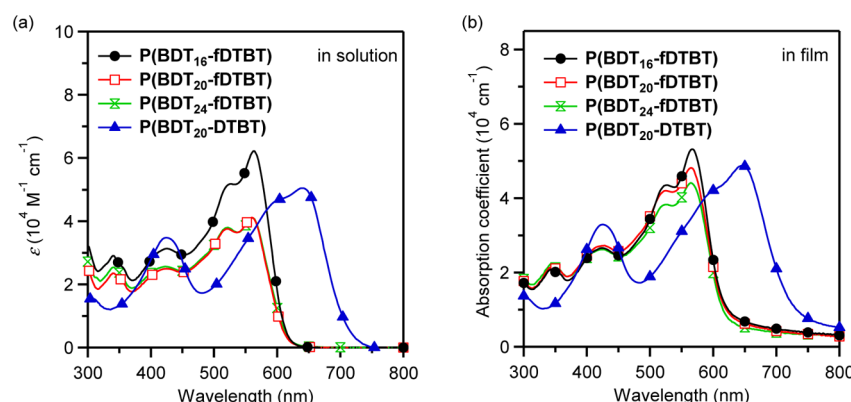


Figure 3. UV-vis absorption spectra at room temperature of $P(BDT_n\text{-}fDTBT)$ ($n = 16, 20$, and 24) and $P(BDT_{20}\text{-}DTBT}$ (a) in solution and (b) in film state.

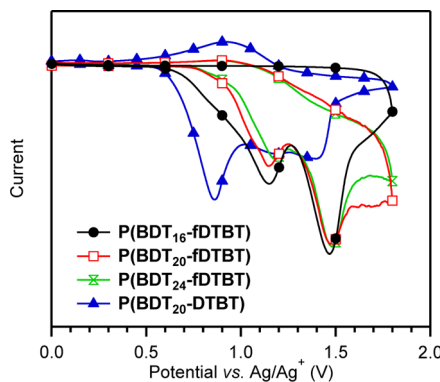


Figure 4. Cyclic voltammograms of P(BDT_n-fDTBT) ($n = 16, 20$, and 24) and P(BDT₂₀-DTBT) films.

peaks around 1.15 and 1.46 V, while P(BDT₂₀-DTBT) displays an irreversible oxidation peak around 0.85 V. Their negative CV scannings were conducted but hard to locate the first reduction peak.

The onset potentials of the first oxidation (E_{ox}) were used to calculate the HOMO energy levels for materials. Based on the facts that the standard energy level of ferrocene/ferrocenium (Fc/Fc⁺) is 4.8 eV below vacuum²⁵ and its redox potential was measured to be 0.07 V under the same conditions, the energy level of the reference electrode (Ag/Ag⁺) engaged in the experiments was calculated to be 4.73 eV. Thus, the polymer HOMO energy level can be derived by the equation

$$\text{HOMO} = -e(E_{ox} + 4.73) \text{ (eV)}$$

In our experiments, the onset oxidation potential (E_{ox}) was determined to be 0.66 V for P(BDT₁₆-fDTBT), 0.77 V for P(BDT₂₀-fDTBT), and 0.79 V for P(BDT₂₄-fDTBT), giving their HOMO levels of -5.39, -5.50, and -5.52 eV, respectively. Meanwhile, the HOMO energy level of P(BDT₂₀-DTBT) was calculated to be -5.26 eV based on its onset oxidation potential of 0.53 V. These data indicate that the HOMO of P(BDT_n-fDTBT) is more negative than that of P(BDT₂₀-DTBT). Since V_{OC} is semiempirically proportional to the energy level difference between the HOMO of donor and the LUMO of acceptor component,²⁶ the deeper HOMO of

P(BDT_n-fDTBT) would be good for their photovoltaic application.

Theoretical Studies. To gain further insight into the structural and electronic properties of P(BDT_n-fDTBT) and P(BDT_n-DTBT), density functional theory (DFT) studies²⁷ have been carried out at the B3LYP²⁸/6-31G** level with the GAUSSIAN09 program.²⁹ For P(BDT_n-fDTBT), a fragment containing one BDT₁₆ unit and two fDTBT units was used as the model. Likewise, for P(BDT_n-DTBT), a fragment containing one BDT₂₀ unit and two DTBT units was used as the model. The optimized structures with the calculated HOMO and LUMO energy levels are shown in Figure 5.

For P(BDT₁₆-fDTBT), the HOMO is mainly distributed on the BDT₁₆ unit (the electronic donor), while the LUMO on the fDTBT unit (the electronic acceptor), suggesting that P(BDT₁₆-fDTBT) is a typical D-A copolymer. The calculated HOMO and LUMO energy levels are -5.124 and -2.446 eV, respectively, giving an energy gap of 2.678 eV. For a model with small methyl groups as side chain, a similar HOMO-LUMO energy gap of 2.694 eV was obtained. This is reasonable since the side chain has a small effect on the HOMO-LUMO gap of the backbone and no interchain interaction was considered in the calculation. The dihedral angles between the BDT₁₆ and fDTBT units are 168.9° (C-C-C-C) and 169.3° (S-C-C-S), suggesting that the polymer backbone is nearly coplanar and thus in good conjugation.

The features of the orbital distributions of P(BDT₂₀-DTBT) are similar as that of P(BDT₁₆-fDTBT). The calculated HOMO energy level is -4.864 eV, while that of LUMO is -2.736 eV, giving an energy gap of 2.128 eV. The comparison of these computed results shows that P(BDT₁₆-fDTBT) has a lower-lying HOMO, which is consistent with the observations in the electrochemical study. The dihedral angles are 173.8° for both C-C-C-C and S-C-C-S between the BDT₂₀ and DTBT units and 179.2° (C-C-C-C) and 179.3° (C-C-C-S) between the thiophene and the benzothiadiazole units. From these dihedral angle data, one may image that the backbone of P(BDT₁₆-fDTBT) adopts a more twisting configuration than that of P(BDT₂₀-DTBT). All the above observations indicate that the structural fusion of DTBT has great impact on the energy level and structural conformation of the polymer.

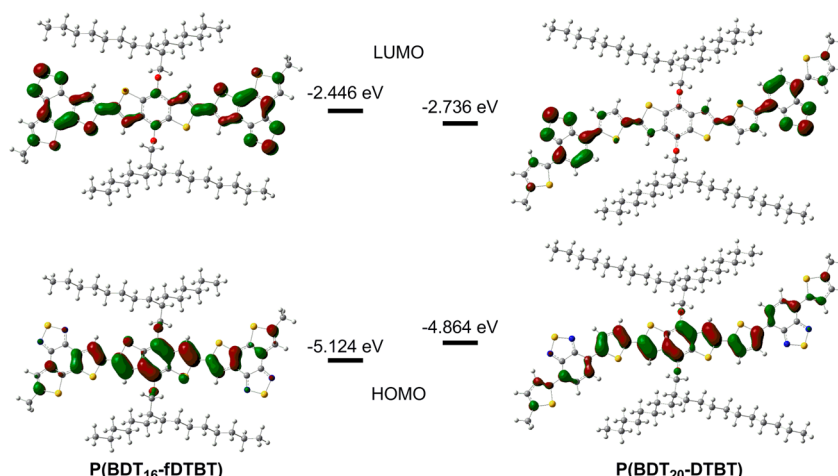


Figure 5. HOMO and LUMO of fragment models of P(BDT₁₆-fDTBT) and P(BDT₂₀-DTBT), depicted at isodensity surface of 0.03 au, calculated at the B3LYP/6-31G** level.

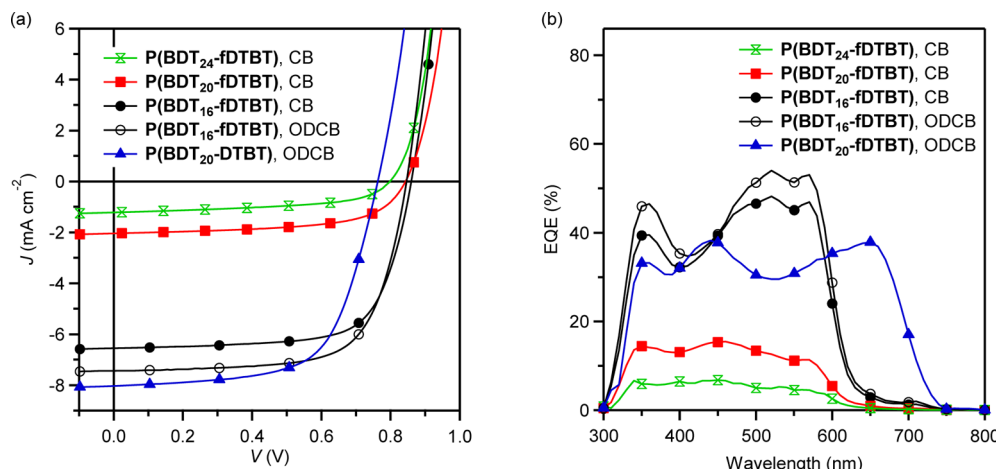


Figure 6. (a) J – V curves and (b) EQE plots of the solar cell devices based on the blend of $P(BDT_n\text{-}fDTBT)$ ($n = 16, 20$, or 24) or $P(BDT_{20}\text{-}DTBT)$ with $PC_{61}\text{BM}$.

Table 2. Device Parameters of the Solar Cells Based on the Blend of $P(BDT_n\text{-}fDTBT)$ ($n = 16, 20$, or 24) or $P(BDT_{20}\text{-}DTBT)$ with $PC_{61}\text{BM}$

polymer	V_{OC} (V)	J_{SC}^e (mA cm ⁻²)	FF (%)	PCE ^f (%)	μ_h (cm ² V ⁻¹ s ⁻¹)
$P(BDT_{24}\text{-}fDTBT)^a$	0.79	1.16 (0.96)	54.0	0.49 (0.56)	4.74×10^{-5}
$P(BDT_{20}\text{-}fDTBT)^a$	0.84	2.04 (1.73)	60.6	1.04 (1.07)	6.85×10^{-5}
$P(BDT_{16}\text{-}fDTBT)^b$	0.86	6.47 (5.78)	69.7	3.88 (3.95)	1.37×10^{-4}
$P(BDT_{16}\text{-}fDTBT)^c$	0.85	7.44 (6.43)	69.0	4.36 (4.50)	1.09×10^{-4}
$P(BDT_{20}\text{-}DTBT)^d$	0.76	8.02 (6.85)	64.4	3.93 (3.98)	1.25×10^{-4}

^aThe polymer/ $PC_{61}\text{BM}$ blending ratio: 1/3 (w/w), solvent: CB. ^bThe polymer/ $PC_{61}\text{BM}$ blending ratio: 1/2 (w/w), solvent: CB. ^cThe polymer/ $PC_{61}\text{BM}$ blending ratio: 1/2 (w/w), solvent: ODCB. ^dThe polymer/ $PC_{61}\text{BM}$ blending ratio: 1/1 (w/w), solvent: ODCB. ^eThe values in parentheses are the calculated J_{SC} from EQE spectra. ^fThe average value, while those in parentheses are the best value for the checked devices.

To find out the origin of the deeper HOMO and higher LUMO of $P(BDT_n\text{-}fDTBT)$ than $P(BDT_n\text{-}DTBT)$, the fragment models Me-fDTBT-Me and Me-DTBT-Me were calculated. The results show that, compared with Me-DTBT-Me, Me-fDTBT-Me has a higher LUMO energy level (-2.085 eV vs -2.505 eV) and a lower HOMO energy level (-5.606 eV vs -5.142 eV). Since the LUMO of the polymer is mainly composed of the LUMO of the fDTBT or DTBT unit, it is reasonable to observe a higher LUMO energy level for $P(BDT_n\text{-}fDTBT)$. Meanwhile, the HOMO of the fDTBT/DTBT unit partially contributes to the HOMO of the polymer. Consequently, $P(BDT_n\text{-}fDTBT)$ has a lower HOMO energy level.

Photovoltaic Properties. The photovoltaic properties of the polymers $P(BDT_n\text{-}fDTBT)$ were investigated with a OSC device structure of ITO/PEDOT:PSS/polymer: $PC_{61}\text{BM}$ /Ca/Al. The active layers were prepared from CB solutions with a total concentration of 20 mg mL⁻¹. The preliminary experiments were carried out to investigate the effect of the polymer/ $PC_{61}\text{BM}$ blending ratio (w/w) from 1/1, 1/2, to 1/3 (Table S1). It was found that $P(BDT_{20}\text{-}fDTBT)$ - and $P(BDT_{24}\text{-}fDTBT)$ -based cells displayed the best photovoltaic efficiency at a blending ratio of 1/3 (w/w), but their performance was much poorer than $P(BDT_{16}\text{-}fDTBT)$ -based cells. Thus, $P(BDT_{16}\text{-}fDTBT)$ -based cells were subjected to further optimization on spin-coating rate. Figure 6a and Table 2 display J – V curves and their parameters, respectively, for the best device of every polymer from CB solution. The highest PCE among the above checked cells was 3.88% with a V_{OC} of 0.86 V, a short-circuit current (J_{SC}) of 6.47 mA cm⁻², and a fill factor (FF) of 69.7%, obtained from $P(BDT_{16}\text{-}fDTBT) / PC_{61}\text{BM}$

device with a blending ratio of 1/2 (w/w) and a spin-coating rate of 1600 rpm. In sharp contrast, the device based on $P(BDT_{24}\text{-}fDTBT)$ having the largest alkyl side chain on BDT unit displayed the worst photoelectric output, with a PCE of only 0.49%. The large decrease in J_{SC} , together with slight decline in V_{OC} and FF, was the main reason for its poor efficiency. For the device based on $P(BDT_{20}\text{-}fDTBT)$, the performance was better than that of $P(BDT_{24}\text{-}fDTBT)$ but worse than that of $P(BDT_{16}\text{-}fDTBT)$. These results were coincided with external quantum efficiency (EQE) spectra of the devices (Figure 6b). The $P(BDT_{16}\text{-}fDTBT)$ -based device exhibited EQE over 40% in the range of 350–600 nm, while those of $P(BDT_{20}\text{-}fDTBT)$ and $P(BDT_{24}\text{-}fDTBT)$ displayed EQE below 15% and 7%, respectively. The above device performance clearly indicates that the side chains of the polymers have great influence on their photovoltaic properties; the smaller the side chain, the better the OPV performance.

Furthermore, it was found that the solvent has great impact on the device performance. When ODCB was used to replace CB, the solar cell based on $P(BDT_{16}\text{-}fDTBT) / PC_{61}\text{BM}$ (1/2, w/w) blend substantially improved J_{SC} value to 7.44 mA cm⁻², while kept V_{OC} and FF virtually intact, resulting in the best average PCE 4.36% among the checked cells. The increased J_{SC} was consistent with the enhanced EQE values for two main photoresponse peaks in EQE spectrum (Figure 6b). Further optimizations with ODCB solvent were carried out on annealing treatment at 80 °C, the addition of 1,8-diiodooctane (DIO) and the replacement of $PC_{61}\text{BM}$ with $PC_{71}\text{BM}$. However, no substantial improvement was observed (Table S1).

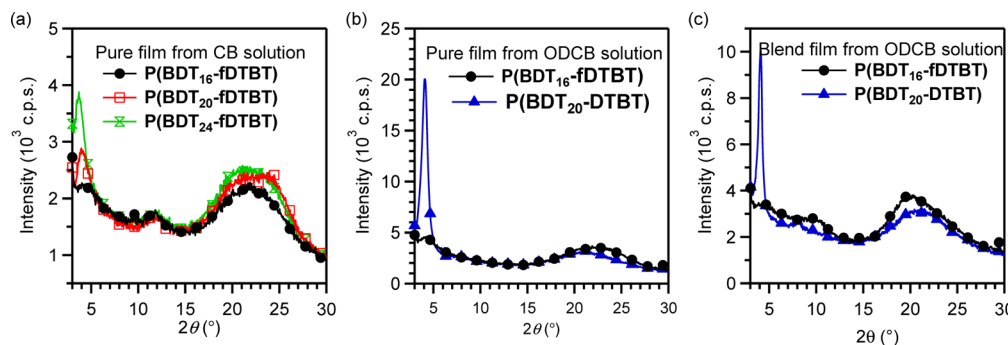


Figure 7. XRD profiles of (a) the pure films of P(BDT_n-fDTBT) ($n = 16, 20$, and 24) casting from their CB solutions, (b) the pure films of P(BDT₁₆-fDTBT) and P(BDT₂₀-DTBT) casting from their ODCB solutions, and (c) the blend films of P(BDT₁₆-fDTBT) and P(BDT₂₀-DTBT) with PC₆₁BM in a weight ratio of $1/2$ and $1/1$, respectively, casting from their ODCB solutions.

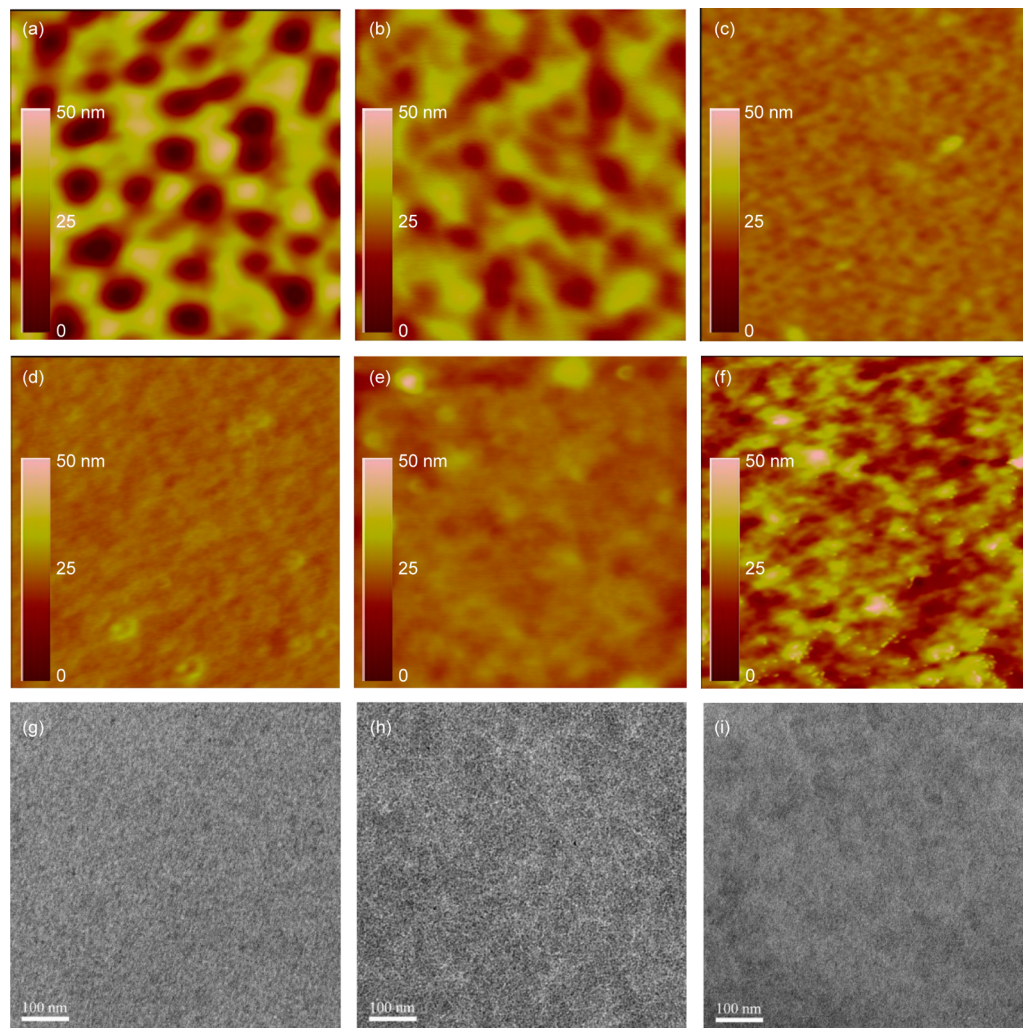


Figure 8. (a–f) Topographical height AFM ($5 \times 5 \mu\text{m}^2$) and (g–i) TEM images of the blend films. (a) P(BDT₂₄-fDTBT)/PC₆₁BM (1/3, w/w) from CB solution, (b) P(BDT₂₀-fDTBT)/PC₆₁BM (1/3, w/w) from CB solution, (c) P(BDT₁₆-fDTBT)/PC₆₁BM (1/2, w/w) from CB solution, (d, g) P(BDT₁₆-fDTBT)/PC₆₁BM (1/2, w/w) from ODCB solution, (e, h) P(BDT₁₆-fDTBT)/PC₆₁BM (1/2, w/w) from ODCB solution with 3% DIO (v/v), and (f, i) P(BDT₂₀-DTBT)/PC₆₁BM (1/1, w/w) from ODCB solution.

The photovoltaic properties of the polymer P(BDT₂₀-DTBT) were investigated in parallel. Because of its soluble nature, ODCB was used as solvent for the device fabrication. As shown in Figure 6a and Table 2, the optimized solar cell showed a J_{SC} of 8.02 mA cm^{-2} , a V_{OC} of 0.76 V , and a FF of 64.4% , giving a PCE of 3.93% . As compared with P(BDT_n-

fDTBT)-based cells, the P(BDT₂₀-DTBT) cell displayed a larger photocurrent. The EQE spectral measurement demonstrated that the photocurrent response of the P(BDT₂₀-DTBT)-based cell extended over 700 nm , much wider than those based on P(BDT_n-fDTBT). This result agrees well with the narrower bandgap nature and wider absorption spectrum of

P(BDT₂₀-DTBT). However, the device of P(BDT₁₆-fDTBT) possessed a larger V_{OC} value than that based on P(BDT₂₀-DTBT), reasonably due to its deeper HOMO energy level. Together with a slightly larger FF value, this larger V_{OC} finally enabled an overpassed performance of the P(BDT₁₆-fDTBT)-based cell to that of P(BDT₂₀-DTBT).

Film Structure, Mobility, and Morphology. In order to get insight into the effect of structural fusion and the side chains on the film structure and morphology, we carried out X-ray diffraction (XRD) first on the pure polymer films and later on their blend films with PC₆₁BM. As shown in Figure 7a, all the pure films of P(BDT_n-fDTBT) casting from their CB solutions displayed three weak diffraction peaks in the ranges of 3°–5°, 10°–15°, and 15°–30°. The first peak is assignable to (100) diffraction of a lamellar structure and gives the information on interlayer distance.³⁰ Because of the different size of the side chains, it is reasonable to observe the *d*-spacing of this peak increased from 2.09 nm for P(BDT₁₆-fDTBT), to 2.22 nm for P(BDT₂₀-fDTBT), and then to 2.38 nm for P(BDT₂₄-fDTBT). The peak in the range of 15°–30° is corresponding to (010) diffraction, which is informative for the interchain π–π stacking distance.³⁰ For all three P(BDT_n-fDTBT) polymer films from CB solutions, this (010) peak was very broad but prominent, with a rough apex around 22° corresponding to a *d*-spacing of 0.40 nm. When the solvent was changed to ODCB, the film of P(BDT₁₆-fDTBT) exhibited a similar XRD diffraction pattern (Figure 7b). In contrast, the film of P(BDT₂₀-DTBT) casting from its ODCB solution showed an intense (100) peak and a weak (200) peak with *d*-spacing of 2.15 and 1.09 nm, respectively, together with a broad and weak (010) peak at *d*-spacing of 0.42 nm. The more intense (100) peak observed for P(BDT₂₀-DTBT) indicates that it adopts more ordered packing structure in film state than P(BDT_n-fDTBT). The further XRD experiment on the polymer/PC₆₁BM blend films (Figure 7c) revealed a similar situation as the pure polymer films, indicating the presence of PC₆₁BM has little influence on the polymer chain packing structure in the film.

To further investigate the effect of the blend film structure on the photovoltaic properties, the hole mobility was detected via the space-charge-limited current (SCLC) method with a hole-only device configuration of ITO/PEDPOT:PSS/polymer:PC₆₁BM/Au.³¹ According to Mott–Gurney law, SCLC theory can be described as

$$J = \frac{9}{8} \varepsilon_0 \varepsilon_r \mu \frac{(V_a - V_{bi})^2}{d^3}$$

where *J* is current density, ε_0 is permittivity of vacuum, ε_r is relative permittivity of the material (for conjugated polymer, ε_r is 3 in general), μ is mobility, V_a is applied voltage, V_{bi} is built-in voltage, and *d* is the thickness of the active film.³² By this method, the hole mobilities for the polymer/PC₆₁BM blend films from chlorobenzene solution based on P(BDT₁₆-fDTBT), P(BDT₂₀-fDTBT), and P(BDT₂₄-fDTBT) were determined to be 1.37×10^{-4} , 6.85×10^{-5} , and 4.74×10^{-5} cm² V⁻¹ s⁻¹, respectively (Table 2). The data clearly show that the hole mobility enhanced when the side chain of the polymer became smaller, which is consistent with the photovoltaic performance of the checked OSC cells. It is valuable to point out that the SCLC hole mobility reaching 10^{-4} cm² V⁻¹ s⁻¹ for a polymer/PC₆₁BM blend film is rather good for photovoltaic performance. When the solvent was replaced with ODCB, no obvious hole mobility change was observed for the P(BDT₁₆-fDTBT)/

PC₆₁BM blend film although in this case the photo-to-electric conversion efficiency increased. Of interest, the blend film of P(BDT₂₀-DTBT)/PC₆₁BM (1/1, w/w) also showed a high mobility (1.25×10^{-4} cm² V⁻¹ s⁻¹), comparable to that of the blend film of P(BDT₁₆-fDTBT)/PC₆₁BM. This indicates the structural fusion of DTBT does not significantly affect the hole transportation in the blend film.

The morphology of the polymer/PC₆₁BM blend films was investigated by atomic force microscopy (AFM). As shown in Figure 8, apparent differences were observed among the checked polymer/PC₆₁BM blend films. In the case of P(BDT₂₄-fDTBT)/PC₆₁BM (1/3, w/w) film spin-coated from a CB solution (Figure 8a), an island–sea structure with a domain size around 200–450 nm was clearly observed. The root-mean-square (RMS) roughness of the film was 9.37 nm. Obviously, such a film was far from ideal for the photovoltaic application and thus resulted in poor photovoltaic performance. When the side chain became smaller, the quality of the morphology gradually improved. The AFM on the blend film of P(BDT₂₀-fDTBT)/PC₆₁BM (1/3, w/w) from a CB solution (Figure 8b) revealed a similar island–sea structure but with rather smaller domain size and RMS value (5.00 nm). The morphology of the blend film of P(BDT₁₆-fDTBT)/PC₆₁BM (1/2, w/w) from CB was completely changed into a percolated biphasic structure with a domain size in several tens of nm (Figure 8c). The film was smooth, with a RMS roughness of 1.53 nm. When the solvent was changed to ODCB, the film further decreased its roughness to 1.24 nm but maintained a percolated biphasic structure with a further smaller domain size. According to the light-to-electric conversion mechanism, such a morphology is ideal for photovoltaics since it could provide a large D/A interface for exciton dissociation, small-enough domains that ensure all the photogenerated excitons have chances to move to D/A interface, and effective transportation pathways for both hole and electron carriers.³³ It was reported DIO can greatly improve the blending film morphology of similar materials.³⁴ But in this work, the addition of 3% DIO made the film more rough, with a RMS roughness of 2.37 nm, thus resulting in decreased performance. For the blend film based on the reference polymer P(BDT₂₀-DTBT) with PC₆₁BM, the morphology became further worse, which appeared to be a biphasic separated structure with a larger domain size in the range of 100–500 nm and a RMS roughness of 5.89 nm. The huge difference in the morphology of the active layer is one of the main reasons for their different photovoltaic performance.

Transmission electron microscopy (TEM) was applied on the blending films of P(BDT₁₆-fDTBT)/PC₆₁BM (1/2, w/w) from ODCB with and without DIO, and the film of P(BDT₂₀-DTBT)/PC₆₁BM (1/1, w/w) to probe their real-space images (Figure 8g–i). The blend film of P(BDT₁₆-fDTBT)/PC₆₁BM from ODCB without DIO appeared homogeneous, with a very small phase separation size. The addition of DIO increased the phase separation size and afforded high contrast areas here and there, implying the aggregation of PC₆₁BM cluster. Such appearance became more obvious for P(BDT₂₀-DTBT)/PC₆₁BM (1/1, w/w) film. The poor blend film microstructure would be one of the reasons for its inferior photovoltaic performance.

3. CONCLUSION

Dithieno[3',2':3,4;2'',3'':5,6]benzo[1,2-*c*][1,2,5]thiadiazole, a fused version of 4,7-dithienyl-2,1,3-benzothiadiazole, was designed, synthesized, and applied for the construction of D–

A copolymers P(BDT_n-fDTBT) with BDT. It has been demonstrated that the side chain on the BDT unit has great impact on the processing and photovoltaic properties of the polymer P(BDT_n-fDTBT) ($n = 8, 10, 12, 16, 20$, and 24). The side chain smaller than 2-butyloctyl ($n \leq 12$) makes the polymer lose processability. In contrast, the side chain larger than 2-octyldodecyl ($n \geq 20$) interferes with $\pi-\pi$ interchain interaction and forms an unfavorable morphology with PC₆₁BM, resulting in low hole mobility and photocurrent. Only in the case of 2-hexyldocyl ($n = 16$), polymer P(BDT_n-fDTBT) shows the best photovoltaic properties with a PCE about 4.36%. More importantly, as compared with nonfused reference polymer P(BDT₂₀-DTBT), the structural fusion of DTBT endows the polymer P(BDT₁₆-fDTBT) with a deeper HOMO level and thus enables the solar cell a larger V_{OC} . Although its bandgap becomes larger, the better morphology and comparable hole mobility for its blend film with PC₆₁BM give the cell device a comparable photocurrent and a slightly larger FF. All these factors influence comprehensively and finally afford P(BDT₁₆-fDTBT), the polymer using the fused DTBT as accepting unit, surpassed photovoltaic performance over the reference polymer with DTBT accepting unit.

4. EXPERIMENTAL SECTION

Measurements and Characterization. ¹H NMR spectra were recorded on a Varian Mercury 300 MHz spectrometer using CDCl₃ as a solvent and tetramethylsilane (TMS) as an internal reference. High-temperature ¹H NMR was performed on a Varian 400-MR 400 MHz spectrometer at 110 °C using tetrachloroethane-d₂ as a solvent. ¹³C NMR spectra were recorded on a DPX 100 MHz spectrometer using CDCl₃ as a solvent and TMS as an internal reference. Electron ionization (EI) mass spectra were measured on an Agilent 5973N mass spectrometer by an electron impact ionization procedure (70 eV). Gel permeation chromatography (GPC) was carried out on a Waters 1515 HPLC instrument equipped with a Waters 2489 UV detector, using CHCl₃ as an eluent or on a PL-GPC 220 instrument equipped with a RI detector, using 1,3,5-trichlorobenzene as an eluent at 150 °C. The molecular weight and polydispersity index (PDI) were calculated based on polystyrene standards. UV-vis absorption spectroscopy was performed on a Hitachi U-3310 spectrophotometer. Cyclic voltammetric (CV) measurements were performed on a CHI 660C instrument using a three-electrode cell with a glassy carbon as working electrode, a platinum wire as counter electrode, and Ag/AgNO₃ as reference electrode. The samples were first casted on a glassy carbon electrode to form a film and then measured in CH₃CN in the presence of 0.1 M Bu₄NPF₆ with a scan rate of 50 mV s⁻¹. Thermogravimetric analysis (TGA) was carried out by a TGA Q500 instrument under N₂ with a temperature rate of 10 °C min⁻¹. Differential scanning calorimetry (DSC) was performed on a Q2000 modulated DSC instrument under N₂ with a heating rate of 10 °C min⁻¹ and a cooling rate of 15 °C min⁻¹. Atomic force microscopy (AFM) was performed on a Veeco instrument Nanoscope IIIa Multimode apparatus by tapping mode with a silicon tip. X-ray diffraction (XRD) was carried out on a PANalytical X'Pert Pro diffractometer with Cu K α beam (40 kV, 40 mA) in $\theta-2\theta$ scans (0.033 Å step size, 30 s/step). Polymer sample films were prepared by drop-casting from their CB or ODCB solutions (5 mg mL⁻¹) onto a quartz plate.

Device Fabrication and Characterization. The solar cell devices were fabricated with a structure of ITO/PEDOT:PSS/active layer/Ca/Al. A thin layer of PEDOT:PSS (Heraeus Clevios P VP. Al 4083) was spin-coated on the top of a well cleaned ITO glass at 4000 rpm and baked at 130 °C for 20 min, affording a thickness of about 30 nm. After transfer into a N₂-filled glovebox, the active layer was spin-coated from a CB or ODCB solution of the polymer and PC₆₁BM (Lumitec LT-8905) with a total weight concentration of 20 mg mL⁻¹. The thermal annealing was performed at 80 °C for 20 min if applied.

Finally, a 10 nm thick Ca layer and a 100 nm thick Al layer were subsequently thermally deposited on the top of the active layer under a high vacuum (10⁻⁵ mbar) through a shadow mask. The effective cell area is 7 mm². Layer thickness was measured on a Veeco Dektak 150 profilometer. Current density–voltage ($J-V$) curves were recorded on a Keithley 2420 source meter. Photocurrent was acquired upon irradiation using an AAA solar simulator (Oriel 94043A, 450 W) with an AM 1.5G filter. The intensity was adjusted to be 100 mW cm⁻² under the calibration with a NREL-certified standard silicon cell (Oriel reference cell 91150). External quantum efficiency (EQE) was detected with a 75 W Xe lamp, Oriel monochromator 7412S, optical chopper, lock-in amplifier and a NREL-calibrated crystalline silicon cell.

Materials. Unless indicated, all commercial reagents were used as received. The solvents for reactions were dehydrated following common methods, tetrahydrofuran (THF), ether, and toluene refluxed over a mixture of Na and benzophenone while chlorobenzene dried over CaH₂ under argon, and freshly distilled prior to use. Benzo[1,2-*b*:4,5-*b'*]dithiophene-4,8-dione³⁵ and 4,7-bis(5-bromo-2-thienyl)-2,1,3-benzothiadiazole (Br-DTBT-Br)³⁶ were synthesized according to the literature methods.

3,3'-Thenil (1). A solution of ethyllithium (57.6 mL, 1.7 M in diethyl ether, 98.0 mmol) was dropwise added into a solution of 3-bromothiophene (8.4 mL, 89.6 mmol) in dry diethyl ether (200 mL) under argon at -78 °C. Then, the reaction mixture was warmed to room temperature and stirred for 50 min. After the mixture was cooled to -78 °C again, 1,4-dimethylpiperazine-2,3-dione (6.37 g, 44.82 mmol) was added, followed by the natural warm-up to room temperature and stirring overnight. The reaction was quenched by a slow addition of aqueous HCl (2 M, 200 mL). Then, the organic layer was collected, washed with water, and dried over anhydrous Na₂SO₄. After filtration, the filtrate was concentrated under reduced pressure. The residue was subjected to silica column chromatography using petroleum ether first and then petroleum ether/CH₂Cl₂ (6:1, v/v) as eluent, allowing to separate 4.40 g of 3,3'-thenil (compound 1) as a yellow solid with a yield of 44.5%. ¹H NMR (300 MHz, CDCl₃) δ (ppm): 8.36 (d, $J = 1.8$ Hz, 2H), 7.70 (d, $J = 5.4$ Hz, 2H), 7.41–7.39 (m, 2H).

Benzo[1,2-*b*:6,5-*b'*]dithiophene-4,5-dione (2). A solution of FeCl₃ (3.75 g, 23.2 mmol) in nitromethane (30 mL) was dropwise added into a vigorously stirred solution of 3,3'-thenil (1) (1.19 g, 5.36 mmol) in dry dichloromethane (250 mL). An argon stream was bubbled through the reaction mixture during the entire reaction. After addition, the mixture was stirred for 3 h and then poured into water (300 mL). The organic layer was separated, washed with saturated NH₄Cl aqueous solution, and dried over anhydrous Na₂SO₄. After filtration, the filtrate was concentrated under reduced pressure, and the residue was subjected to silica column chromatography using CHCl₃ as eluent, allowing to separate 0.92 g of compound 2 as a black solid in a yield of 78.0%. ¹H NMR (300 MHz, CDCl₃) δ (ppm): 7.51 (d, $J = 5.1$ Hz, 2H), 7.22 (d, $J = 5.1$ Hz, 2H).

Benzo[1,2-*b*:6,5-*b'*]dithiophene-4,5-diamine (4). A solution of compound 2 (2.10 g, 9.5 mmol), NH₂OH-HCl (5.29 g, 76.1 mmol), and pyridine (22.4 mL) in EtOH (224 mL) was heated under reflux for 20 h. After the mixture was cooled to room temperature, the solvent was removed under reduced pressure. After the addition of water (150 mL), the precipitate was collected and dried, affording the crude dioxime compound 3 (2.34 g), which was used for the next step without further purification. Then, compound 3 was dissolved in anhydrous EtOH (300 mL). After the addition of 10% Pd/C (2.30 g), the mixture was flushed with argon and heated to reflux. A solution of 40 mL of N₂H₄·H₂O in 80 mL of anhydrous EtOH was dropwise injected into the above mixture over 30 min. After refluxed overnight, the hot reaction mixture was passed through a pad of Celite via suction, and the Celite was thoroughly washed with boiling EtOH. The filtrate was concentrated, and the residue was subjected to silica column chromatography using dichloromethane/ethanol (9/1, v/v) as eluent, allowing to separate 1.49 g of compound 4 as a gray-white solid in a yield of 71.0% for two steps. ¹H NMR (300 MHz, CDCl₃) δ

(ppm): 7.55 (d, $J = 5.4$ Hz, 2H), 7.40 (d, $J = 5.4$ Hz, 2H), 4.83 (s, 4H).

Dithieno[3',2':3,4;2",3":5,6]benzo[1,2-c][1,2,5]thiadiazole (fDTBT). A mixture of diamine compound 4 (1.49 g, 6.77 mmol), CH_2Cl_2 (40 mL), and Et_3N (3.76 mL, 27.1 mmol) was stirred until the diamine compound 4 was dissolved. After the dropwise addition of thionyl chloride (0.96 mL, 13.5 mmol), the mixture was refluxed for 5 h. Then, the mixture was concentrated under reduced pressure and added with H_2O (80 mL). After pH was adjusted to 2 by concentrated HCl, the mixture was extracted with CH_2Cl_2 (3×70 mL). The organic phase was combined, washed with H_2O (2×50 mL), and dried over Na_2SO_4 . After filtration, the filtrate was concentrated, and the residue was subjected to silica column chromatography using petroleum ether/ CH_2Cl_2 (1/1, v/v) as eluent, allowing to separate 0.90 g of fDTBT as a yellow solid in a yield of 53.5%. ^1H NMR (300 MHz, CDCl_3) δ (ppm): 8.05 (d, $J = 5.4$ Hz, 2H), 7.56 (d, $J = 5.4$ Hz, 2H). ^{13}C NMR (100 MHz, CDCl_3) δ (ppm): 150.6, 135.5, 129.0, 125.4, 124.3. EI MS: 248 (100%).

5,8-Dibromodithieno[3',2':3,4;2",3":5,6]benzo[1,2-c][1,2,5]thiadiazole (Br-fDTBT-Br). To a mixture of compound fDTBT (0.40 g, 1.68 mmol), chloroform (14 mL), and acetic acid (14.5 mL) was dropwise added with the solution of bromine (0.19 mL, 3.70 mmol) in chloroform (1.9 mL) at 0 °C. After further addition of chloroform (50 mL), the mixture was refluxed for 5 h. Then, the reaction mixture was cooled to room temperature and filtrated. The filtrate cake was collected, dried, recrystallized from *o*-dichlorobenzene, allowing to afford 0.55 g of compound Br-fDTBT-Br as a yellow needle solid in a yield of 84.1%. ^1H NMR (400 MHz, $\text{C}_2\text{D}_2\text{Cl}_4$, 110 °C) δ (ppm): 8.01 (s, 2H). EI MS: 406 (100%). Anal. Calcd for $\text{C}_{10}\text{H}_2\text{Br}_2\text{N}_2\text{S}_3$: C, 29.57; H, 0.50; N, 6.90. Found: C, 29.73; H, 0.41; N, 7.14.

4,8-Di(2-hexyl)decyloxybenzo[1,2-b;3,4-b']dithiophene (BDT₁₆). Benzo[1,2-b:4,5-b']dithiophene-4,8-dione (0.56 g, 2.5 mmol), zinc powder (0.41 g, 6.4 mmol), and water (7.5 mL) were put into a 100 mL flask under the protection of argon. Then NaOH (1.50 g, 37.5 mmol) was added into the mixture. The mixture was well stirred and heated to reflux for 1 h. During the reaction, the color of the mixture changed from yellow to red and then to orange. Afterward, 2-hexyldecyl bromide (2.35 g, 7.7 mmol) and a catalytic amount of tetrabutylammonium bromide (0.05 g, 0.15 mmol) were added into the flask. After being refluxed for 2 h, the reaction mixture was poured into cold water and extracted with diethyl ether. The organic layer was combined and dried over anhydrous Na_2SO_4 . After filtration, the filtrate was concentrated under reduced pressure, and the residue was subjected to silica column chromatography using hexane as eluent, allowing to separate 1.20 g of compound BDT₁₆ as colorless oil in a yield of 71.6%. ^1H NMR (300 MHz, CDCl_3) δ (ppm): 7.47 (d, $J = 5.7$ Hz, 2H), 7.36 (d, $J = 5.7$ Hz, 2H), 4.16 (br, 4H), 1.86 (br, 2H), 1.61 (br, 4H), 1.53–1.26 (m, 44H), 0.89 (br, 12H).

4,8-Di(2-ethyl)hexyloxybenzo[1,2-b;3,4-b']dithiophene (BDT₈). Compound BDT₈ was synthesized as colorless oil in a yield of 80.9% following the similar method of BDT₁₆. ^1H NMR (300 MHz, CDCl_3) δ (ppm): 7.48 (d, $J = 5.4$ Hz, 2H), 7.36 (d, $J = 5.4$ Hz, 2H), 4.14 (d, $J = 4.5$ Hz, 4H), 1.85–1.26 (m, 18H), 0.98 (t, $J = 5.4$ Hz, 6H), 0.88 (t, $J = 5.4$ Hz, 6H).

4,8-Di(3,7-dimethyl)octyloxybenzo[1,2-b;3,4-b']dithiophene (BDT₁₀). Compound BDT₁₀ was synthesized as colorless oil in a yield of 95.5% following the similar method of BDT₁₆. ^1H NMR (300 MHz, CDCl_3) δ (ppm): 7.48 (d, $J = 5.7$ Hz, 2H), 7.36 (d, $J = 5.7$ Hz, 2H), 4.32 (br, 4H), 1.97–1.15 (m, 20H), 0.97 (d, $J = 6.3$ Hz, 6H), 0.88 (t, $J = 6.6$ Hz, 12H).

4,8-Di(2-butyl)octyloxybenzo[1,2-b;3,4-b']dithiophene (BDT₁₂). Compound BDT₁₂ was synthesized as colorless oil in a yield of 79.6% following the similar method of BDT₁₆. ^1H NMR (300 MHz, CDCl_3) δ (ppm): 7.46 (d, $J = 5.7$ Hz, 2H), 7.37 (d, $J = 5.7$ Hz, 2H), 4.17 (br, 4H), 1.86 (br, 2H), 1.63 (br, 4H), 1.53–1.26 (m, 28H), 0.90 (m, 12H).

4,8-Di(2-octyl)dodecyloxybenzo[1,2-b;3,4-b']dithiophene (BDT₂₀). Compound BDT₂₀ was synthesized as colorless oil in a yield of 49.2% following the similar method of BDT₁₆. ^1H NMR (300 MHz, CDCl_3) δ (ppm): 7.46 (d, $J = 5.7$ Hz, 2H), 7.36 (d, $J = 5.7$ Hz, 2H),

4.16 (d, $J = 5.1$ Hz, 4H), 1.89–1.82 (m, 2H), 1.62–1.52 (m, 4H), 1.52–1.27 (m, 60H), 0.90–0.86 (m, 12H).

4,8-Di(2-decyl)tetradecyloxybenzo[1,2-b;3,4-b']dithiophene (BDT₂₄). Compound BDT₂₄ was synthesized as colorless oil in a yield of 51.6% following the similar method of BDT₁₆. ^1H NMR (300 MHz, CDCl_3) δ (ppm): 7.46 (d, $J = 5.7$ Hz, 2H), 7.36 (d, $J = 5.7$ Hz, 2H), 4.16 (d, $J = 5.1$ Hz, 4H), 1.89–1.82 (m, 2H), 1.62–1.27 (m, 80H), 0.90–0.86 (t, $J = 6.6$ Hz, 12H).

2,6-Bis(trimethyltin)-4,8-di(2-hexyl)decyloxybenzo[1,2-b;3,4-b']dithiophene (Sn-BDT₁₆-Sn). Compound BDT₁₆ (0.70 g, 1.04 mmol) and dry THF (20 mL) were added into a flask under an inert atmosphere. The solution was cooled down to –78 °C and dropwise added with *n*-butyllithium (2.93 mL, 1.6 M in *n*-hexane, 4.69 mmol). After being warmed to room temperature and stirred for 2 h, the reaction mixture was cooled to –78 °C again. Then, trimethyltin chloride (5.0 mL, 1 M in *n*-hexane, 5.0 mmol) was added, and the reaction mixture was allowed to naturally warm to room temperature and stirred overnight. After quenched with water (100 mL), the mixture was extracted with ether for three times. The combined organic layer was washed with water and dried over anhydrous Na_2SO_4 . After filtration, the filtrate was concentrated under reduced pressure, and the residue was recrystallized from isopropanol to give 0.45 g of compound Sn-BDT₁₆-Sn as white needle in a yield of 43.3%. ^1H NMR (300 MHz, CDCl_3) δ (ppm): 7.51 (s, 2H), 4.18 (d, $J = 3.9$ Hz, 4H), 1.86 (br, 2H), 1.64–1.29 (m, 48H), 0.90–0.87 (m, 12H), 0.44 (s, 18H). ^{13}C NMR (100 MHz, CDCl_3) δ (ppm): 143.20, 140.32, 133.82, 132.87, 127.93, 75.88, 39.18, 31.95, 31.40, 30.16, 29.81, 29.70, 29.39, 27.06, 27.00, 22.71, 22.68, 14.12, –8.40. Anal. Calcd for $\text{C}_{48}\text{H}_{86}\text{O}_2\text{S}_2\text{Sn}_2$: C, 57.84; H, 8.70. Found: C, 57.78; H, 8.70.

2,6-Bis(trimethyltin)-4,8-di(2-ethyl)hexyloxybenzo[1,2-b;3,4-b']dithiophene (Sn-BDT₈-Sn). Compound Sn-BDT₈-Sn was synthesized as white needle in a yield of 88.7% following the similar method of Sn-BDT₁₆-Sn. ^1H NMR (300 MHz, CDCl_3) δ (ppm): 7.52 (s, 2H), 4.19 (d, $J = 3.9$ Hz, 4H), 1.84–1.41 (m, 18H), 1.03 (t, $J = 6.0$ Hz, 6H), 0.95 (t, $J = 6.0$ Hz, 6H), 0.45 (s, 18H). ^{13}C NMR (100 MHz, CDCl_3) δ (ppm): 143.22, 140.35, 133.83, 132.87, 127.95, 75.60, 40.65, 30.52, 29.23, 23.89, 23.16, 14.17, 11.34, –8.38. Anal. Calcd for $\text{C}_{32}\text{H}_{54}\text{O}_2\text{S}_2\text{Sn}_2$: C, 49.76; H, 7.05. Found: C, 49.56; H, 6.97.

2,6-Bis(trimethyltin)-4,8-di(3,7-dimethyl)octyloxybenzo[1,2-b;3,4-b']dithiophene (Sn-BDT₁₀-Sn). Compound Sn-BDT₁₀-Sn was synthesized as white needle in a yield of 61.8% following the similar method of Sn-BDT₁₆-Sn. ^1H NMR (300 MHz, CDCl_3) δ (ppm): 7.51 (s, 2H), 4.39–4.28 (m, 4H), 1.97–1.19 (m, 20H), 0.99 (t, $J = 6.9$ Hz, 6H), 0.87 (t, $J = 6.6$ Hz, 12H), 0.44 (s, 18H). ^{13}C NMR (100 MHz, CDCl_3) δ (ppm): 143.10, 140.46, 133.95, 132.93, 127.98, 71.89, 39.28, 37.62, 37.31, 29.75, 27.97, 24.71, 22.71, 22.61, 19.72, –8.34. Anal. Calcd for $\text{C}_{36}\text{H}_{62}\text{O}_2\text{S}_2\text{Sn}_2$: C, 52.19; H, 7.54. Found: C, 52.32; H, 7.55.

2,6-Bis(trimethyltin)-4,8-di(2-butyl)octyloxybenzo[1,2-b;3,4-b']dithiophene (Sn-BDT₁₂-Sn). Compound Sn-BDT₁₂-Sn was synthesized as white needle in a yield of 73.8% following the similar method of Sn-BDT₁₆-Sn. ^1H NMR (300 MHz, CDCl_3) δ (ppm): 7.51 (s, 2H), 4.18 (d, $J = 3.9$ Hz, 4H), 1.86 (br, 2H), 1.67 (br, 4H), 1.56–1.26 (m, 28H), 0.97–0.90 (m, 12H), 0.44 (s, 18H). ^{13}C NMR (100 MHz, CDCl_3) δ (ppm): 143.20, 140.33, 133.81, 132.88, 127.93, 75.87, 39.16, 31.95, 31.39, 31.09, 29.81, 29.25, 27.00, 23.16, 22.71, 14.18, 14.13, –8.41. Anal. Calcd for $\text{C}_{40}\text{H}_{70}\text{O}_2\text{S}_2\text{Sn}_2$: C, 54.31; H, 7.98. Found: C, 54.49; H, 8.02.

2,6-Bis(trimethyltin)-4,8-di(2-octyl)dodecyloxybenzo[1,2-b;3,4-b']dithiophene (Sn-BDT₂₀-Sn). Compound Sn-BDT₂₀-Sn was synthesized as white needle in a yield of 82.1% following the similar method of Sn-BDT₁₆-Sn. ^1H NMR (300 MHz, CDCl_3) δ (ppm): 7.51 (s, 2H), 4.17 (d, $J = 3.9$ Hz, 4H), 1.85 (br, 2H), 1.64–1.27 (m, 64H), 0.89 (t, $J = 6.3$ Hz, 12H), 0.44 (s, 18H). ^{13}C NMR (100 MHz, CDCl_3) δ (ppm): 143.20, 140.30, 133.82, 132.86, 127.93, 75.91, 39.18, 31.92, 31.39, 30.17, 29.74, 29.71, 29.67, 29.39, 29.36, 27.05, 22.68, 14.11, –8.39. Anal. Calcd for $\text{C}_{56}\text{H}_{102}\text{O}_2\text{S}_2\text{Sn}_2$: C, 60.65; H, 9.27. Found: C, 61.04; H, 9.24.

2,6-Bis(trimethyltin)-4,8-di(2-decyl)tetradecyloxybenzo[1,2-b;3,4-b']dithiophene (Sn-BDT₂₄-Sn). Compound Sn-BDT₂₄-Sn was synthesized as white needle in a yield of 90.0% following the similar method

of Sn-BDT₁₆-Sn. ¹H NMR (300 MHz, CDCl₃) δ (ppm): 7.51 (s, 2H), 4.17 (d, *J* = 3.9 Hz, 4H), 1.86 (br, 2H), 1.64–1.26 (m, 80H), 0.86 (t, *J* = 5.1 Hz, 12H), 0.44 (s, 18H). ¹³C NMR (100 MHz, CDCl₃) δ (ppm): 143.20, 140.30, 133.82, 132.86, 127.94, 75.90, 39.18, 31.91, 31.39, 30.17, 29.75, 29.71, 29.67, 29.35, 27.06, 22.67, 14.11, –8.38. Anal. Calcd for C₆₄H₁₁₈O₂S₂Sn₂: C, 62.95; H, 9.74. Found: C, 62.77; H, 9.67.

General Procedure for Synthesis of Polymers P(BDT_n-fDTBT) and P(BDT_n-DTBT). To a two-necked flask was added dibromide monomer (0.1 mmol), bis(trimethylstannyl)-substituted monomer Sn-BDT_n-Sn (0.1 mmol), and dry toluene (15 mL). After being degassed by argon bubbling for 10 min, the solution of Pd(PPh₃)₄ (1.1 mg, 0.001 mmol) in dry toluene (1 mL) was added. The reaction mixture was degassed again via argon bubbling for 20 min. Then, the reaction mixture was heated to 110 °C and stirred for 48 h. After being cooled to room temperature, the reaction mixture was poured into 100 mL of methanol, allowing to precipitate the crude polymer. After filtration, the crude product was subjected to Soxhlet extraction with methanol, acetone, hexane, chloroform, and chlorobenzene in sequence. The corresponding fraction that extracted the polymer was evaporated to dryness and further dried in vacuum for 1 day to get the final product. The yields for all polymers were about 80–90%.

■ ASSOCIATED CONTENT

S Supporting Information

¹H NMR, ¹³C NMR, EI mass spectra, and summarized table for the parameters of all checked solar cell devices. This material is available free of charge via the Internet at <http://pubs.acs.org>.

■ AUTHOR INFORMATION

Corresponding Authors

*E-mail meichy@sioc.ac.cn (C.-Y.M.).

*E-mail liyuxue@sioc.ac.cn (Y.-X.L.).

*E-mail liws@mail.sioc.ac.cn (W.-S.L.).

Notes

The authors declare no competing financial interest.

■ ACKNOWLEDGMENTS

This work was supported by National Natural Science Foundation of China (Nos. 20974119, 90922019, 21074147, and 21121062) and Chinese Academy of Sciences.

■ REFERENCES

- (a) Gunes, S.; Neugebauer, H.; Sariciftci, N. S. *Chem. Rev.* **2007**, *107*, 1324–1338. (b) Cheng, Y.-J.; Yang, S.-H.; Hsu, C.-S. *Chem. Rev.* **2009**, *109*, 5868–5923. (c) Chen, J.; Cao, Y. *Acc. Chem. Res.* **2009**, *42*, 1709–1718. (d) Li, G.; Zhu, R.; Yang, Y. *Nat. Photonics* **2012**, *6*, 153–161.
- (a) Liang, Y.; Xu, Z.; Xia, J.; Tsai, S.-T.; Wu, Y.; Li, G.; Ray, C.; Yu, L. *Adv. Mater.* **2010**, *22*, E135–E138. (b) Huo, L.; Zhang, S.; Guo, X.; Xu, F.; Li, Y.; Hou, J. *Angew. Chem., Int. Ed.* **2011**, *50*, 9697–9702. (c) He, Z.; Zhong, C.; Su, S.; Xu, M.; Wu, H.; Cao, Y. *Nat. Photonics* **2012**, *6*, 591–595.
- (3) Chu, T.-Y.; Lu, J.; Beaupré, S.; Zhang, Y.; Pouliot, J.-R.; Wakim, S.; Zhou, J.; Leclerc, M.; Li, Z.; Ding, J.; Tao, Y. *J. Am. Chem. Soc.* **2011**, *133*, 4250–4253.
- (4) Zhou, H.; Yang, L.; Stuart, A. C.; Price, S. C.; Liu, S.; You, W. *Angew. Chem., Int. Ed.* **2011**, *50*, 2995–2998.
- (5) Amb, C. M.; Chen, S.; Graham, K. R.; Subbiah, J.; Small, C. E.; So, F.; Reynolds, J. R. *J. Am. Chem. Soc.* **2011**, *133*, 10062–10065.
- (6) Chang, C.-Y.; Cheng, Y.-J.; Hung, S.-H.; Wu, J.-S.; Kao, W.-S.; Lee, C.-H.; Hsu, C.-S. *Adv. Mater.* **2012**, *24*, 549–553.
- (7) (a) Halls, J. M.; Walsh, C. A.; Greenham, N. C.; Marseglia, E. A.; Friend, R. H.; Moratti, S. C.; Holmes, A. B. *Nature* **1995**, *376*, 498–500. (b) Yu, G.; Gao, J.; Hummelen, J. C.; Wudl, F.; Heeger, A. J. *Science* **1995**, *270*, 1789–1791. (c) Meskers, S. C. J.; van Hal, P. A.; Spiering, A. J. H.; Hummelen, J. C.; van der Meer, A. F. G.; Janssen, R. A. *J. Phys. Rev. B* **2000**, *61*, 9917–9920.
- (8) (a) Li, G.; Shrotriya, V.; Huang, J. S.; Yao, Y.; Moriarty, T.; Emery, K.; Yang, Y. *Nat. Mater.* **2005**, *4*, 864–868. (b) Ma, W.; Yang, C.; Gong, X.; Lee, K.; Heeger, A. J. *Adv. Funct. Mater.* **2005**, *15*, 1617–1622.
- (9) (a) Jenekhe, S. A.; Lu, L.; Alam, M. M. *Macromolecules* **2001**, *34*, 7315–7324. (b) Zhu, Y.; Champion, R. D.; Jenekhe, S. A. *Macromolecules* **2006**, *39*, 8712–8719. (c) Zhan, X.; Zhu, D. *Polym. Chem.* **2010**, *1*, 409–419. (d) Ye, H.; Li, W.; Li, W.-S. *Chin. J. Org. Chem.* **2012**, *32*, 266–283.
- (10) Zhou, H.; Yang, L.; You, W. *Macromolecules* **2012**, *45*, 607–632.
- (11) (a) Svensson, M.; Zhang, F.; Veenstra, S. C.; Verhees, W. J. H.; Hummelen, J. C.; Kroon, J. M.; Inganäs, O.; Andersson, M. R. *Adv. Mater.* **2003**, *15*, 988–991. (b) Zhou, Q.; Hou, Q.; Zheng, L.; Deng, X.; Yu, G.; Cao, Y. *Appl. Phys. Lett.* **2004**, *84*, 1653–1655. (c) Slooff, L. H.; Veenstra, S. C.; Kroon, J. M.; Moet, D. J. D.; Sweelissen, J.; Koetsje, M. M. *Appl. Phys. Lett.* **2007**, *90*, 143506–143508. (d) Chen, M.-H.; Hou, J.; Hong, Z.; Yang, G.; Sista, S.; Chen, L.-M.; Yang, Y. *Adv. Mater.* **2009**, *21*, 4238–4242.
- (12) Chen, Y.-C.; Yu, C.-Y.; Fan, Y.-L.; Hung, L.-I.; Chen, C.-P.; Ting, C. *Chem. Commun.* **2010**, *46*, 6503–6505.
- (13) Cheng, Y.-J.; Cheng, S.-W.; Chang, C.-Y.; Kao, W.-S.; Liao, M.-H.; Hsu, C.-S. *Chem. Commun.* **2012**, *48*, 3203–3205.
- (14) Cheng, Y.-J.; Chen, C.-H.; Lin, Y.-S.; Chang, C.-Y.; Hsu, C.-S. *Chem. Mater.* **2011**, *23*, 5068–5075.
- (15) Blouin, N.; Michaud, A.; Leclerc, M. *Adv. Mater.* **2007**, *19*, 2295–2300.
- (16) Park, S. H.; Roy, A.; Beaupré, S.; Cho, S.; Coates, N.; Moon, J. S.; Moses, D.; Leclerc, M.; Lee, K.; Heeger, A. J. *Nat. Photonics* **2009**, *3*, 297–302.
- (17) Boudreault, P. L. T.; Michaud, A.; Leclerc, M. *Macromol. Rapid Commun.* **2007**, *28*, 2176–2179.
- (18) Zhou, E.; Nakamura, M.; Nishizawa, T.; Zhang, Y.; Wei, Q.; Tajima, K.; Yang, C.; Hashimoto, K. *Macromolecules* **2008**, *41*, 8302–8305.
- (19) (a) Lu, J.; Liang, F.; Drolet, N.; Ding, J.; Tao, Y.; Movileanu, R. *Chem. Commun.* **2008**, *44*, 5315–5317. (b) Zhou, E.; Yamakawa, S.; Zhang, Y.; Zhang, Y.; Tajima, K.; Yang, C.; Hashimoto, K. *J. Mater. Chem.* **2009**, *19*, 7730–7737. (c) Zhou, E.; Cong, J.; Yamakawa, S.; Wei, Q.; Nakamura, M.; Tajima, K.; Yang, C.; Hashimoto, K. *Macromolecules* **2010**, *43*, 2873–2879.
- (20) Zheng, Q.; Jung, B. J.; Sun, J.; Katz, H. E. *J. Am. Chem. Soc.* **2010**, *132*, 5394–5404.
- (21) Zhou, E.; Cong, J.; Hashimoto, K.; Tajima, K. *Macromolecules* **2013**, *46*, 763–768.
- (22) Tovar, J. D.; Rose, A.; Swager, T. M. *J. Am. Chem. Soc.* **2002**, *124*, 7762–7769.
- (23) Liang, Y.; Feng, D.; Wu, Y.; Tsai, S.-T.; Li, G.; Ray, C.; Yu, L. *J. Am. Chem. Soc.* **2009**, *131*, 7792–7799.
- (24) (a) Liang, Y.; Wu, Y.; Feng, D.; Tsai, S.-T.; Son, H.-J.; Li, G.; Yu, L. *J. Am. Chem. Soc.* **2009**, *131*, 56–57. (b) Zhang, G.; Fu, Y.; Zhang, Q.; Xie, Z. *Chem. Commun.* **2010**, *46*, 4997–4999.
- (25) Zhang, J.; Cai, W.; Huang, F.; Wang, E.; Zhong, C.; Liu, S.; Wang, M.; Duan, C.; Yang, T.; Cao, Y. *Macromolecules* **2011**, *44*, 894–901.
- (26) Dennler, G.; Scharber, M. C.; Brabec, C. J. *Adv. Mater.* **2009**, *21*, 1323–1338.
- (27) (a) Hohenberg, P.; Kohn, W. *Phys. Rev.* **1964**, *136*, B864–B871. (b) Kohn, W.; Sham, L. *J. Phys. Rev.* **1965**, *140*, A1133–A1138.
- (28) (a) Becke, A. D. *J. Chem. Phys.* **1993**, *98*, 5648–5652. (b) Lee, C.; Yang, W.; Parr, R. G. *Phys. Rev.* **1988**, *B37*, 785–789.
- (29) Frisch, M. J.; Trucks, G. W.; Schlegel, H. B.; Scuseria, G. E.; Robb, M. A.; Cheeseman, J. R.; Scalmani, G.; Barone, V.; Mennucci, B.; Petersson, G. A.; Nakatsuji, H.; Caricato, M.; Li, X.; Hratchian, H. P.; Izmaylov, A. F.; Bloino, J.; Zheng, G.; Sonnenberg, J. L.; Hada, M.; Ehara, M.; Toyota, K.; Fukuda, R.; Hasegawa, J.; Ishida, M.; Nakajima, T.; Honda, Y.; Kitao, O.; Nakai, H.; Vreven, T.; Montgomery, A., Jr.; Peralta, J. E.; Ogliaro, F.; Bearpark, M.; Heyd, J. J.; Brothers, E.; Kudin,

K. N.; Staroverov, V. N.; Kobayashi, R.; Normand, J.; Raghavachari, K.; Rendell, A.; Burant, J. C.; Iyengar, S. S.; Tomasi, J.; Cossi, M.; Rega, N.; Millam, J. M.; Klene, M.; Knox, J. E.; Cross, J. B.; Bakken, V.; Adamo, C.; Jaramillo, J.; Gomperts, R.; Stratmann, R. E.; Yazev, O.; Austin, A. J.; Cammi, R.; Pomelli, C.; Ochterski, J. W.; Martin, R. L.; Morokuma, K.; Zakrzewski, V. G.; Voth, G. A.; Salvador, P.; Dannenberg, J. J.; Dapprich, S.; Daniels, A. D.; Farkas, O.; Foresman, J. B.; Ortiz, J. V.; Cioslowski, J.; Fox, D. J. *Gaussian 09, Revision A.01*; Gaussian, Inc.: Wallingford, CT, 2009.

(30) Hwang, Y.-J.; Ren, G.; Murari, N. M.; Jenekhe, S. A. *Macromolecules* **2012**, *45*, 9056–9062.

(31) (a) Fu, Y.; Cha, H.; Lee, G. -Y.; Moon, B. J.; Park, C. E.; Park, T. *Macromolecules* **2012**, *45*, 3004–3009. (b) Duan, R.; Ye, L.; Guo, X.; Huang, Y.; Wang, P.; Zhang, S.; Zhang, J.; Huo, L.; Hou, J. *Macromolecules* **2012**, *45*, 3032–3038.

(32) Yang, C.-M.; Liao, H.-H.; Horng, S.-F.; Meng, H.-F.; Tseng, S.-R.; Hsu, C.-S. *Synth. Met.* **2008**, *158*, 25–28.

(33) Dong, L.; Li, W.; Li, W.-S. *Nanoscale* **2011**, *3*, 3447–3461.

(34) Huang, Y.; Liu, F.; Guo, X.; Zhang, W.; Gu, Y.; Zhang, J.; Han, C. C.; Russell, T. P.; Hou, J. *Adv. Energy Mater.* **2013**, *3*, 930–937.

(35) Hou, J.; Park, M.-H.; Zhang, S.; Yao, Y.; Chen, L.-M.; Li, J.-H.; Yang, Y. *Macromolecules* **2008**, *41*, 6012–6018.

(36) Kim, J.; Park, S. H.; Cho, S.; Jin, Y.; Kim, J.; Kim, I.; Lee, J. S.; Kim, J. H.; Woo, H. Y.; Lee, K.; Suh, H. *Polymer* **2010**, *51*, 390–396.